Original Article

A Fuzzy MPPT Based Voltage Regulator Integrated Asymmetrical Multi-Level Inverter Standalone PV Source

Rampalli Jagan¹, Bhaskar Kanna²

 1,2 Department of Electrical and Electronics Engineering, JNTUH University College of Engineering Science and Technology, Kukatpally, Hyderabad, Telangana, India.

¹Corresponding Author: jagan.gnit@gmail.com

Received: 15 May 2025 Revised: 25 September 2025 Accepted: 07 October 2025 Published: 31 October 2025

Abstract - The replacement of conventional energy sources with renewable alternatives has become a key strategy to mitigate global warming. Among these, PV systems are highly promising due to their flexible deployment and relatively low initial cost. However, PV systems produce fluctuating power and unstable DC voltage since their output depends directly on solar irradiation. To effectively harness PV power, this work integrates a fuzzy logic-based MPPT voltage regulator with an asymmetrical multilevel inverter connected to a standalone PV array. The proposed system employs four PV modules operating at different voltage levels, configured with an asymmetrical 31-level inverter. These voltage levels are combined by a level generator to produce 15 distinct voltage steps, which are then inverted using a four-switch full bridge. A comparative study is conducted between the conventional MPPT P&O method and the FL-based MPPT regulator. The results highlight the superior performance of the fuzzy MPPT approach in achieving optimal control for the standalone PV inverter, as demonstrated by higher extracted power amplitude and reduced tracking time.

Keywords - Photo Voltaic (PV), Maximum Power Point Tracking (MPPT), Fuzzy logic, Perturb and Observe (P&O), Fuzzy Logic (FL), Asymmetrical multi-level inverter.

1. Introduction

Future power generation in most countries is expected to shift from fossil fuels, such as coal and nuclear, toward renewable energy sources. However, renewable sources inherently suffer from intermittency, as their output depends on variable natural factors like solar irradiation, wind, and tidal activity. These fluctuations directly affect the voltage and current stability of renewable systems [1]. To address this, renewable sources are often integrated in parallel with the grid, sharing power with the load while remaining synchronized to the grid voltage [2]. Achieving such synchronization, however, requires complex inverter control strategies. In periods of renewable power deficit, the grid seamlessly supplies the required load demand without voltage disturbances [3]. In remote areas where grid access is unavailable due to distance or infrastructure limitations, standalone renewable systems become necessary. In such cases, conventional diesel generators that rely on fossil fuels should be replaced with clean, renewable alternatives [4].

Installing standalone renewable energy systems presents significant challenges, as the variability of natural resources directly affects power generation [5]. To ensure reliable operation, power extracted from renewable sources must be regulated at stable voltage levels, thereby maintaining a quality supply to the load. PV panels are widely adopted for ease of deployment in remote areas as they generate electricity from solar irradiation. These panels can be configured in series or parallel and in different combinations to meet the desired power and voltage requirements [6]. The PV output is then fed into a conventional boost converter, which provides voltage boosting and stabilization [7]. By using the inverter, the controlled direct voltage is converted to alternating voltage. At the inverter output, an LC filter is used to smooth the output and produce a sinusoidal voltage. A boost converter is used to extract the maximum power using the traditional Perturb and Observe MPPT method.

Conventional renewable power extraction and conversion methods often result in slow tracking response, voltage drops, and significant power losses, thereby reducing overall efficiency. In conventional multi-level voltage generation circuits, configurations such as cascaded H-bridge, diodeclamped, and capacitor-clamped converters are commonly employed. These designs require multiple power switches, and as the voltage levels increase, the number of switches also

grows. A higher switch count results in greater switching losses and increased harmonic distortion due to resonance. Additionally, the overall cost of the inverter rises with the increased number of components. Consequently, as switching losses escalate with more switches, the efficiency of these converters decreases. To overcome these limitations, traditional converters and controllers must be replaced with advanced circuit topologies and intelligent control strategies.

In this work, a 31-level asymmetrical inverter is proposed, designed to operate without the need for an LC filter. The inverter input is derived from four PV modules configured at different voltage levels [8]. Each PV module is equipped with an individual boost converter regulated by an MPPT-based voltage controller, ensuring stable and precise output voltage levels. The complete outline of the proposed PV-integrated inverter topology is shown in Figure 1.

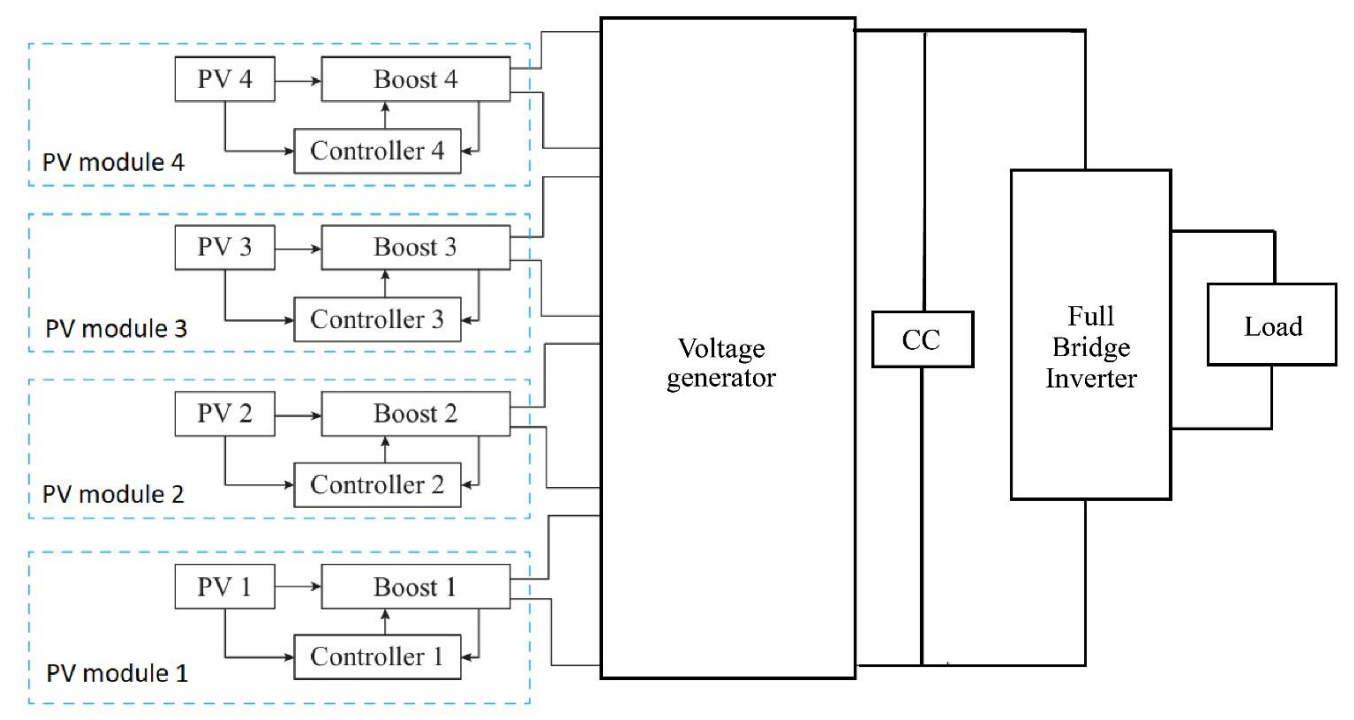


Fig. 1 Structure of the proposed multi-level inverter with PV source

As illustrated in Figure 1, the four Photovoltaic segments are connected to a voltage level generator that produces a multi-level DC output. The generator consists of four sets of MOSFET—diode circuits, configured to generate 15 distinct voltage levels. This is achieved through asymmetrical voltage magnitudes of the PV modules, which are maintained at Vdc, 2Vdc, 4Vdc, and 8Vdc for modules 1 through 4, respectively. Each boost converter regulates its corresponding PV module to ensure these reference voltages are achieved, enabling the voltage level generator to create the 15-level DC output.

This 15-level DC voltage is then converted into a 31-level AC waveform by a four-switch full-bridge inverter, achieved through alternate diagonal switching of the bridge switches. The high-quality 31-level output significantly reduces harmonics, eliminating the need for an LC filter and thereby minimizing losses and voltage drops [9]. Consequently, the stabilized AC output can be directly supplied to the load without filtering, ensuring maximum power transfer from the PV modules. The conventional P&O algorithm is used to control each boost converter to extract maximum power. To further enhance power extraction and improve voltage

regulation, a fuzzy logic-based MPPT voltage regulator is integrated into each PV module in the advanced design [10].

The paper is arranged with Section 1 presenting the proposed standalone PV-based asymmetrical 31-level inverter system. Section 2 presents the design and operation of the converter, including detailed current conduction paths and the implementation of the conventional P&O-based MPPT voltage regulator for the boost converter. Section 3 describes the FL-based MPPT voltage regulator and the rule-based tables used for its modelling. Section 4 provides the simulation results of the projected system, including a relative analysis of the P&O and FL MPPT techniques. Section 5 concludes the paper by validating the results and identifying the optimal MPPT strategy. The conclusion is followed by a list of references cited throughout the work.

2. 31-Level Inverter Design

The 31-level asymmetrical inverter is initially composed of four switches and four diodes arranged to generate multiple voltage levels. The four MOSFET switches in the voltage-level generation stage produce 15 distinct voltage levels,

corresponding to the reference voltages of the PV modules. As previously stated, the PV modules are regulated to supply Vm, 2*Vm, 4*Vm, and 8*Vm for modules 1 through 4, respectively [11]. These 15 voltage levels are then processed by a four-switch full-bridge inverter, which alternately directs them into positive and negative cycles to form the complete 31-level output. The overall circuit configuration of the projected asymmetrical inverter is illustrated in Figure 2.

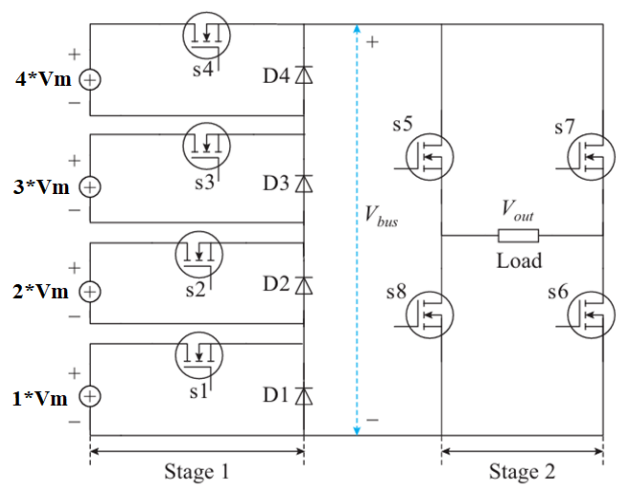


Fig. 2 31-level asymmetrical inverter circuit

As shown in Figure 2, when a MOSFET switch is turned ON, the corresponding diode becomes reverse-biased and switches OFF [12]. The sequential operation of switches S1–S4 generates the required voltage levels in accordance with the switching states, which are given in Table 1.

Table 1. Switching states of the voltage level generator

S1	S2	S3	S4	Voltage level
OFF	OFF	OFF	OFF	0
ON	OFF	OFF	OFF	1*Vm
OFF	ON	OFF	OFF	2*Vm
ON	ON	OFF	OFF	3*Vm
OFF	OFF	ON	OFF	4*Vm
ON	OFF	ON	OFF	5*Vm
OFF	ON	ON	OFF	6*Vm
ON	ON	ON	OFF	7*Vm
OFF	OFF	OFF	ON	8*Vm
ON	OFF	OFF	ON	9*Vm
OFF	ON	OFF	ON	10*Vm
ON	ON	OFF	ON	11*Vm
OFF	OFF	ON	ON	12*Vm
ON	OFF	ON	ON	13*Vm
OFF	ON	ON	ON	14*Vm
ON	ON	ON	ON	15*Vm

According to the switching table, the voltage level generator operates to produce the DC bus voltage (Vbus), consisting of 15 discrete levels during each half cycle of the reference signal. The PV module voltages are regulated at the

desired levels (Vm, 2*Vm, 4*Vm, and 8*Vm) through MPPT-based voltage controllers [13]. For a purely resistive load, the generated voltage levels remain stable without spikes, as the load cannot store energy. However, when the load includes an inductive component, energy stored in the inductor can cause voltage overshoots during the zero-voltage state in each half cycle.

In this condition, the stored charge in the inductor discharges back toward the DC bus during the zero-voltage interval, creating large voltage spikes. Such overshoots can potentially damage both the load and the components of the asymmetrical inverter. To mitigate this issue, a capacitor compensator circuit is employed at the inverter's DC bus [14]. The compensator consists of multiple capacitors, which are selectively switched ON based on the load's reactive power (Qload) demand. The configuration of the capacitor compensator, comprising six capacitors (C1–C6) connected in parallel with series switches (Sc1–Sc6), is illustrated in Figure 3.

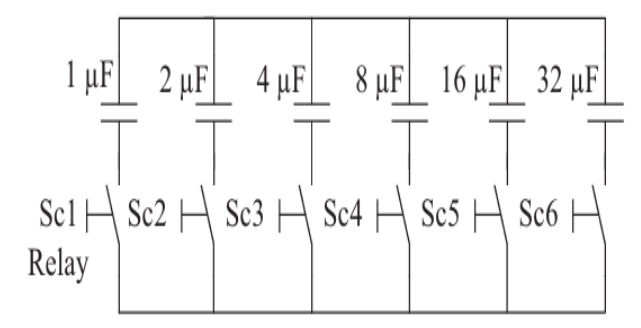


Fig. 3 Circuit structure of the capacitor compensator device

As shown in Figure 3, the capacitor compensator consists of six capacitors, where the capacitance value doubles successively for each parallel branch. The operation of switches Sc1–Sc6 is determined by the Q_{load} of the load, the RMS load voltage (V_rms), and the supply frequency (f). Based on these component values, the required compensation capacitance is calculated as:

$$C = \frac{Q_{load}}{2\pi f V_{rms}^2} \tag{1}$$

Based on the calculated capacitance, each switch is triggered accordingly, with a maximum of 63 μF that can be connected to the DC bus [15]. This controlled switching is essential to prevent overcompensation, which could distort the voltage waveform and introduce harmonics. For extreme power abstraction from the PVs, the initial MPPT method employed is the conventional P&O technique. The P&O-based voltage regulator operates using three measured variables: PV panel voltage (Vpv), PV panel current (Ipv), and Vdc (boost converter output voltage) [16]. The conventional P&O-MPPT algorithm is illustrated by using a flowchart shown in Figure 4.

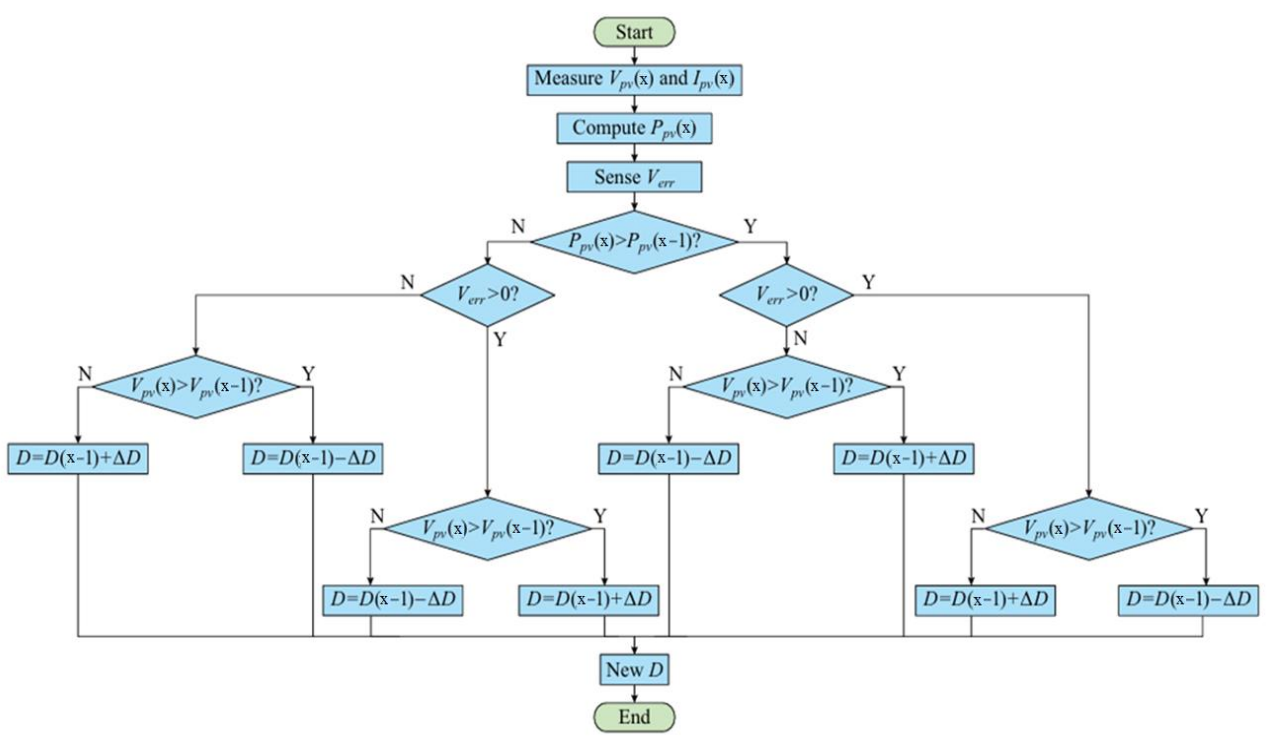


Fig. 4 P&O-based voltage regulator MPPT technique

According to the flowchart, the duty ratio of the BC switch is controlled—either increased or decreased—based on the comparison between the current and former values of voltage and power. The conditions governing the increment or decrement of the duty ratio are expressed as follows:

$$P_{nv}(x) = V_{nv}(x) * I_{nv}(x)$$
 (2)

Here, Vpv(x) and Ipv(x) represent the instantaneous values of the PV panel voltage and current, respectively. Using these measurements, the instantaneous PV power Ppv(x) is calculated. The error voltage (Verr) is then achieved by comparing the reference voltage (Vref) with the boost converter output voltage (Vo), expressed as:

$$V_{err} = V_{ref} - V_o \tag{3}$$

The duty ratio (D) is now adjusted by an incremental value (ΔD), which is either added to or subtracted from the previous duty ratio D(x –1). The expressions for determining the present duty ratio, based on the calculated variables, are given as follows:

$$\begin{split} D &= D(x-1) + \Delta D \\ \left\{ \begin{aligned} &If \ P_{pv}(x) > P_{pv}(x-1), \ V_{err} > 0, V_{pv}(x) < V_{pv}(x-1) \\ &If \ P_{pv}(x) > P_{pv}(x-1), \ V_{err} < 0, V_{pv}(x) > V_{pv}(x-1) \\ &If \ P_{pv}(x) < P_{pv}(x-1), \ V_{err} > 0, V_{pv}(x) > V_{pv}(x-1) \\ &If \ P_{pv}(x) < P_{pv}(x-1), \ V_{err} < 0, V_{pv}(x) < V_{pv}(x-1) \end{aligned} \right. \end{split}$$

$$D = D(x-1) - \Delta D$$

$$\begin{cases}
If P_{pv}(x) > P_{pv}(x-1), V_{err} > 0, V_{pv}(x) > V_{pv}(x-1) \\
If P_{pv}(x) > P_{pv}(x-1), V_{err} < 0, V_{pv}(x) < V_{pv}(x-1) \\
If P_{pv}(x) < P_{pv}(x-1), V_{err} > 0, V_{pv}(x) < V_{pv}(x-1) \\
If P_{pv}(x) < P_{pv}(x-1), V_{err} < 0, V_{pv}(x) > V_{pv}(x-1)
\end{cases}$$
(5)

The past values Ppv(x - 1) and Vpv(x - 1) are obtained using a delay or memory block applied to the present measured values.

The calculated duty ratio (D) is then compared with a sawtooth or triangular carrier signal, typically operating in the frequency range of (5–10) kHz, to generate the switching states for the boost converter.

Through this relative comparison, the boost converter regulates its output voltage to match the desired reference value. To achieve improved tracking of the duty ratio and enhance power extraction, the conventional P&O-based voltage regulator MPPT is replaced with a fuzzy logic-based MPPT regulator. The design methodology of the proposed fuzzy MPPT technique is presented in the following section.

3. Fuzzy-based MPPT Voltage Regulator

The FL-based voltage regulator MPPT method employs two fuzzy sets to determine the D of BC. Similar to the P&O method, it requires the measured signals Vpv, Ipv, and Verr to regulate the duty ratio [17]. A schematic flow of the FL-based MPPT controller is presented in Figure 5.

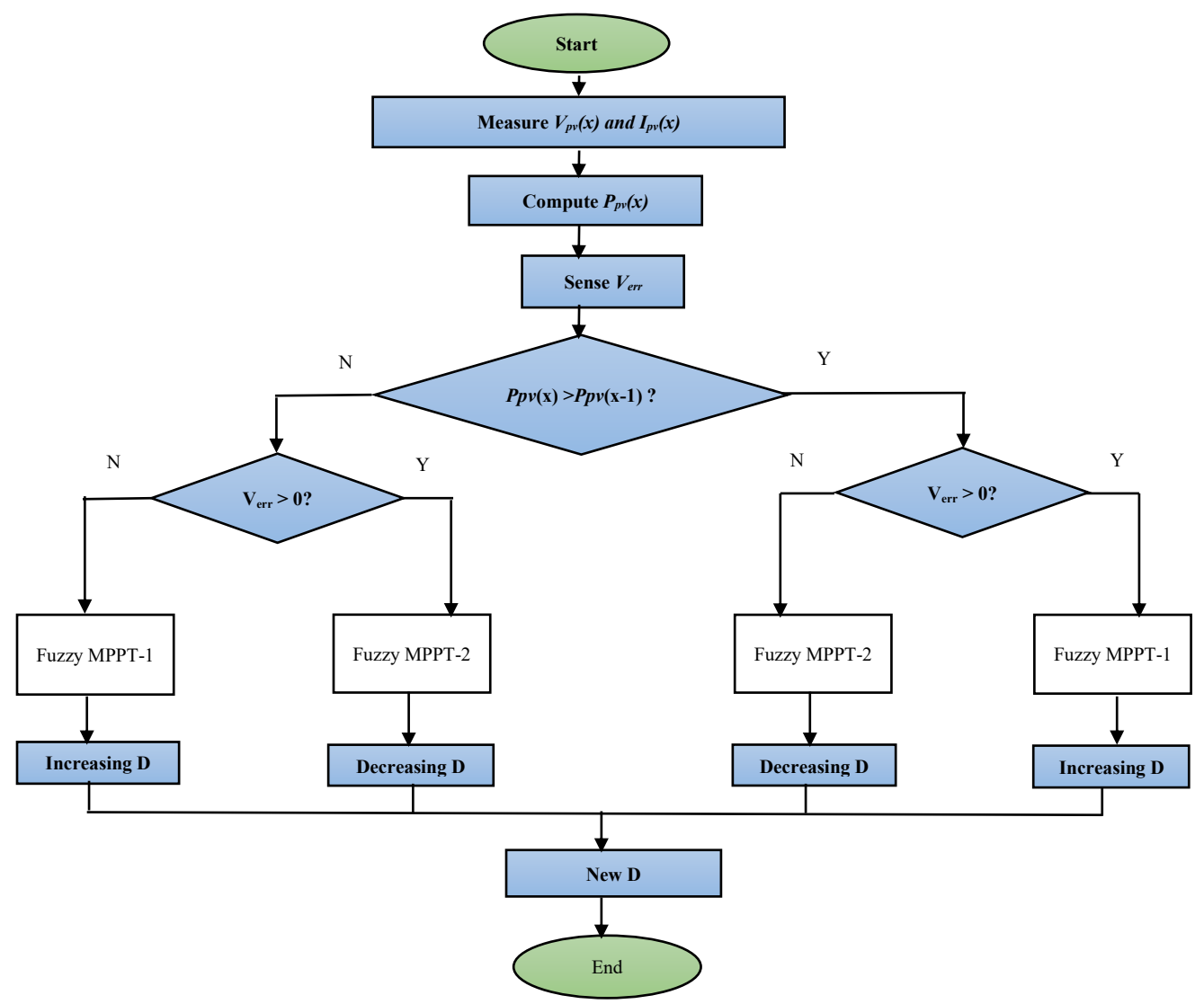


Fig. 5 Fuzzy-based voltage regulator MPPT flow chart

Each fuzzy set consists of two input variables and one output variable. The input variables are the change in power (dP) and the change in voltage (dV), while the output variable is the change in duty ratio (cD). These variables are

represented by membership functions, distributed across regions according to their minimum and maximum values [18]. The Membership Functions (MFs) for the fuzzy MPPT variables are illustrated in Figure 6.

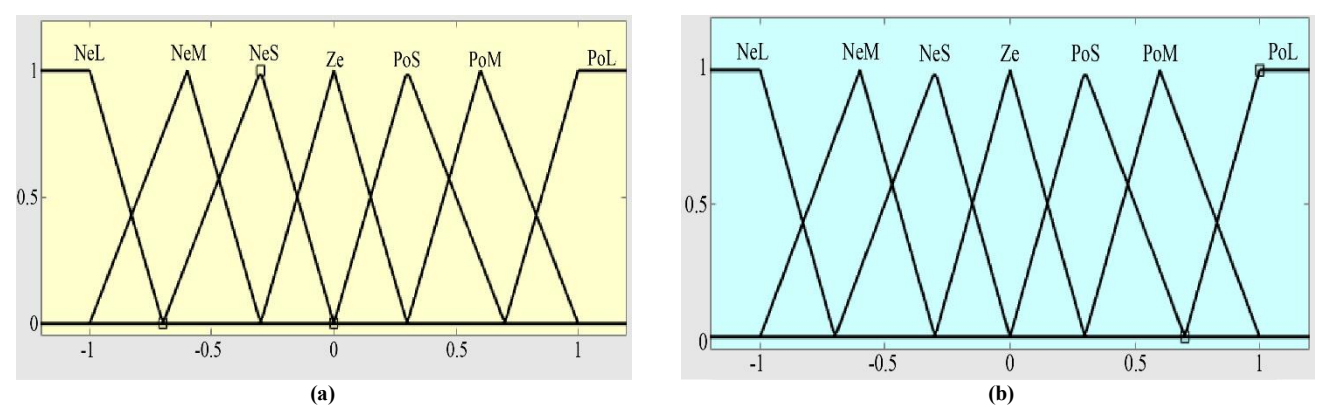


Fig. 6 Membership functions (a) Input variables (dP and dV) MFs, and (b) Output variable (cD) MFs.

In this system, all the variables, including input and output, are represented with seven linguistic membership functions, named as Negative Large (NeL), Negative Medium (NeM), Negative Small (NeS), Zero(ze), Positive Small (PoS), Positive Medium (PoM) and Positive Large (PoL) [19]. All membership functions are distributed over a normalized range of -1 to 1, utilizing triangular-shaped MFs. The input values are computed based on the present and past measurements of power and voltage, expressed as:

$$dP = P(x) - P(x - 1) \tag{6}$$

$$dV = V(x) - V(x - 1) \tag{7}$$

Here, P(x) and V(x) represent the present measured values of PV power and voltage, while P(x-1) and V(x-1) denote their corresponding past values [20]. The output of the fuzzy module is derived from a 49-rule base, constructed using the seven membership functions defined for each variable. Two separate rule sets are developed, corresponding to the flowchart shown in Figure 5, and are applied to the two fuzzy MPPT modules (MPPT-1 and MPPT-2). Based on the given rule table, the fuzzy sets are defined using *If-Then* rules within the fuzzy tool and subsequently exported to the model.

Table 2. MPPT 1 rule-based

Tuble 2. Will I I Tule bused									
cD		dP							
		NeL	NeM	NeS	Ze	PoS	PoM	PoL	
	NeL	NeL	NeL	NeM	Ze	PoM	PoL	PoL	
	NeM	NeL	NeM	NeM	Ze	PoM	PoM	PoL	
	NeS	NeL	NeM	NeS	Ze	PoS	PoM	PoL	
dV	Ze	Ze	Ze	Ze	Ze	Ze	Ze	Ze	
	PoS	PoS	PoS	PoS	Ze	NeS	NeM	NeL	
uv	PoM	PoM	PoM	PoS	Ze	NeS	NeM	NeL	
	PoL	PoL	PoL	PoM	Ze	NeM	NeL	NeL	

Table 3. MPPT 2 rule-based

cD		dP						
		NeL	NeM	NeS	Ze	PoS	PoM	PoL
	NeL	PoL	PoL	PoM	Ze	NeM	NeL	NeL
	NeM	PoL	PoM	PoM	Ze	NeM	NeM	NeL
	NeS	PoL	PoM	PoS	Ze	NeS	NeM	NeL
dV	Ze	Ze	Ze	Ze	Ze	Ze	Ze	Ze
	PoS	NeL	NeM	NeS	Ze	PoS	PoS	PoS
	PoM	NeL	NeM	NeS	Ze	PoS	PoM	PoM
	PoL	NeL	NeL	NeM	Ze	PoM	PoL	PoL

Using the measured and calculated values of Vpv, Ppv, and Verr, the duty ratio is updated through the output variable cD, which regulates the boost converter's output voltage.

4. Result Analysis

The proposed circuit and its control modules were simulated in MATLAB/Simulink to analyse the system performance. For circuit implementation, blocks from the

Electrical subset of the Simscape library were utilized, while the controller was modelled using blocks from the Commonly Used Blocks and Control subsets. Simulation results were obtained in the form of graphical plots for various circuit measurements to validate the performance and enable comparative analysis. The comparison was conducted for systems of identical ratings but with different MPPT controllers. The ratings of the circuit model considered for the analysis are given in Table 4.

Table 4. System parameters

Table 4. System parameters					
Name of the module	Components				
	Manufacturer: SunPower SPR-76R- BLK-U				
PV panels	Vmp = 13.5V, Imp = 5.65A, Voc = 16.2V, Isc = 6.02A.				
Boost converter	Lb = 5mH, Cin = 100μ F, Co = 4000μ F, Right = $1m\Omega$, Rdiode = $0.1m\Omega$.				
P&O MPPT	Vdc_ref1 = 21, Vdc_ref2 = 42, Vdc_ref3 = 64, Vdc_ref4 = 168, Dint = 0.3, MPPT gain = 1, fc = 5kHz.				
Asymmetrical inverter	Rmosfet = $10\text{m}\Omega$, Rdiode = $0.1\text{m}\Omega$,				
Capacitor compensator	C1 = $1\mu F$, C2 = $2\mu F$, C3 = $4\mu F$, C4 = $8\mu F$, C5 = $16\mu F$, C6 = $32\mu F$, Rswitch = $1m\Omega$.				
Load	Rload = 2kW, Lload = 500VAR				
Fuzzy MPPT	Type: Mamdani, MFs = 7, Rules 49 dP range = -1.2 to 1.2, dV range = -1.2 to 1.2, cD range = -1.2 to 1.2.				

The above parameters were incorporated into the simulation models for both the P&O and fuzzy MPPT techniques. Simulations were carried out for a duration of 3 seconds under both constant and varying irradiation conditions to enable comparative analysis. All results are presented as time-domain plots, with the variations in measured quantities illustrated in the following Figures.

4.1. Case 1: Constant Irradiation for All the PV Arrays

In this case, the solar irradiation for all PV modules is operated at a constant maximum value of $1000~W/m^2$ to validate the circuit characteristics. Figure 7 illustrates the output characteristics of all PV panels under constant irradiation conditions.

As shown in Figure 7, the recorded voltages of the PV modules are 15 V for Segment 1, 28 V for Segment 2, 52 V for Segment 3, and 102 V for Segment 4. These voltages are boosted by the respective converters, operated under MPPT-based voltage regulation, to 21 V, 42 V, 84 V, and 168 V, respectively. The boosted outputs are then processed by the voltage level generator, producing the multi-level voltages illustrated in Figure 8.

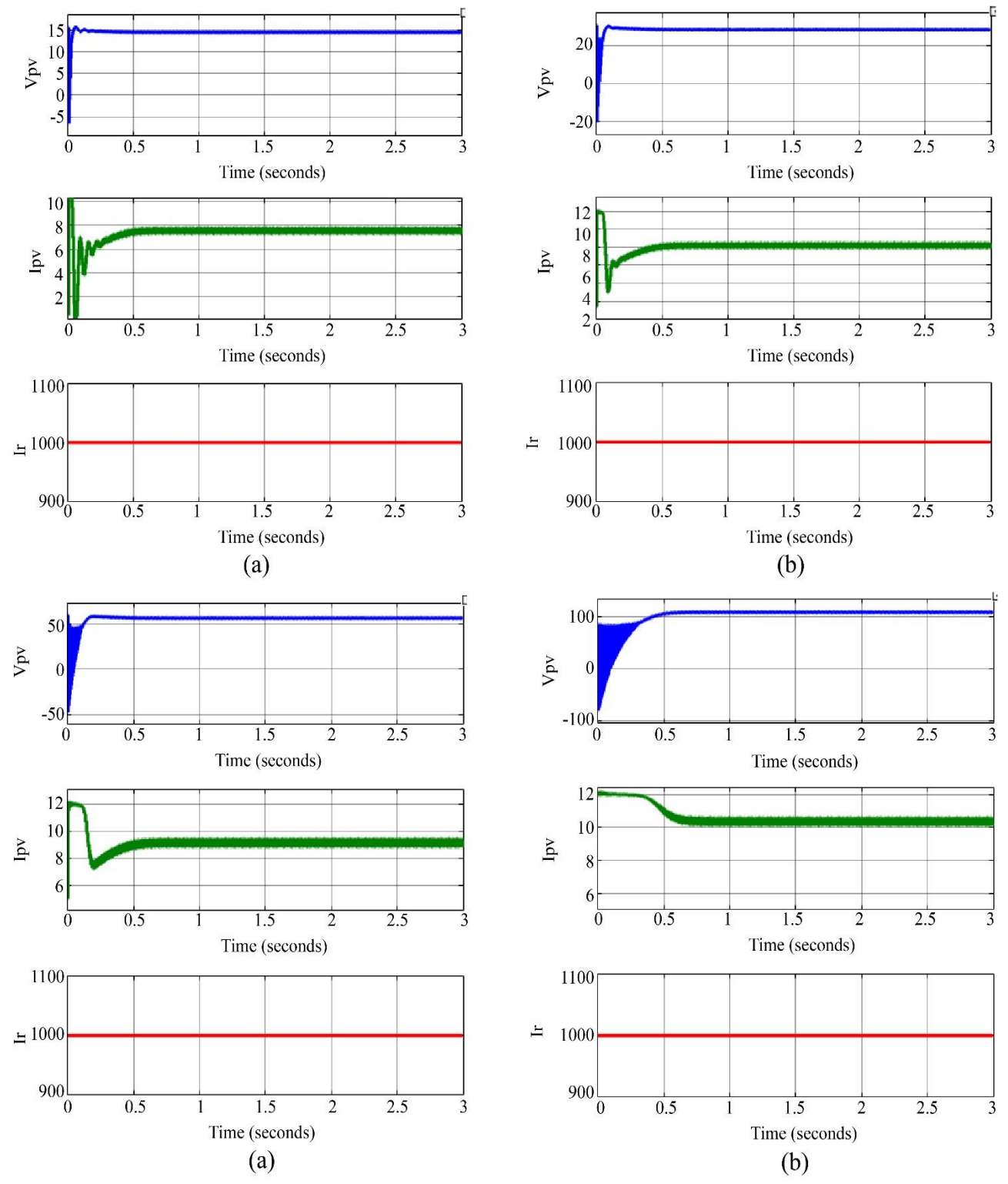


Fig. 7 PV characteristics of (a) PV Segment 1, (b) PV Segment 2, (c) PV Segment 3, and (d) PV Segment 4 for constant irradiation.

As shown in Figure 8, fifteen voltage levels are generated, ranging from 0 V to 320 V, corresponding to the boosted outputs of the PV modules. These voltage levels are determined based on the single-phase RMS reference voltage

of 230 V. The unidirectional DC bus voltage is then alternately inverted in each half cycle by the four-switch inverter. Figure 9 presents the inverter output voltage waveform under a purely resistive load.

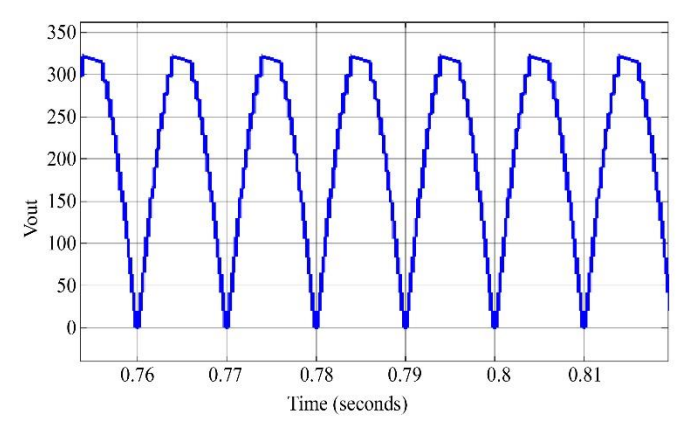


Fig. 8 DC bus voltage

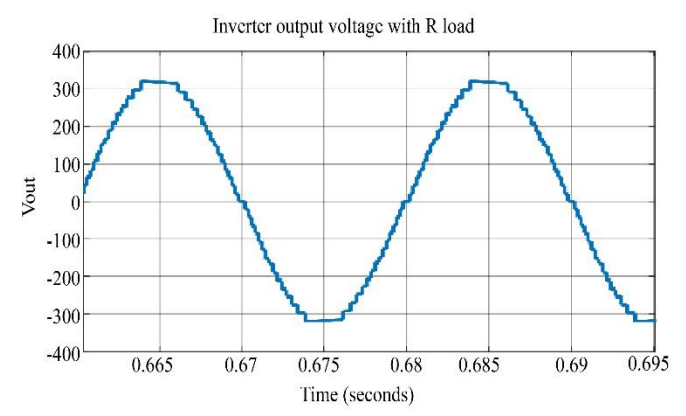


Fig. 9 Output voltage of the inverter with only a resistive load

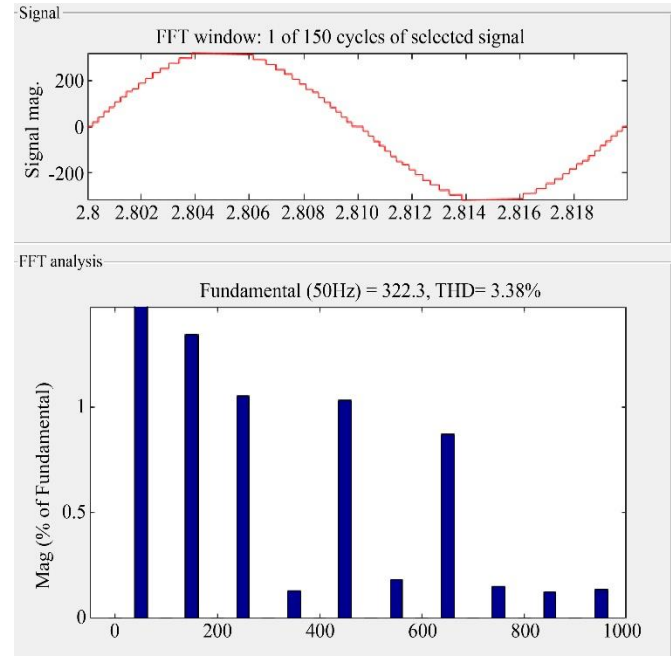


Fig. 10 FFT analysis of inverter voltage with only a resistive load

The inverter output voltage is evaluated using the FFT analysis tool to determine the Total Harmonic Distortion (THD) of the 31-level waveform. As shown in Figure 10, the

THD is measured at 3.38% when the inverter operates with a purely resistive load. In the next case, the load is modified to a resistive–inductive (RL) combination, which activates the capacitor compensator for reactive power compensation and suppression of voltage spikes. The corresponding inverter output voltage with the RL load is presented in Figure 11.

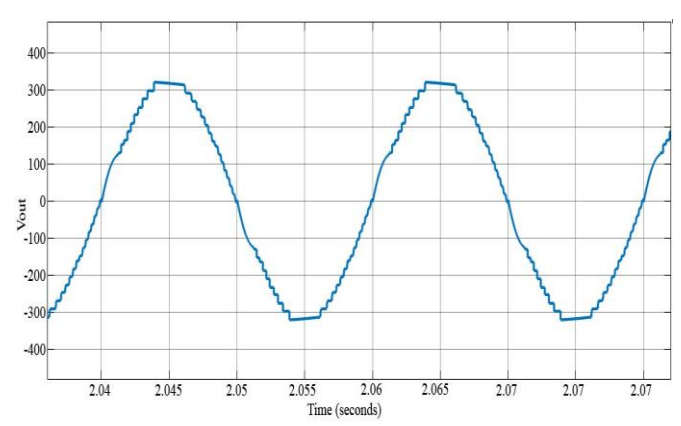


Fig. 11 Output voltage of the inverter with resistive and inductive load

As shown in Figure 11, the inverter voltage waveform experiences slight distortion due to reverse conduction. Nevertheless, the voltage pattern is maintained to generate 31 distinct levels, closely resembling a sinusoidal shape. The corresponding FFT analysis of the inverter output voltage under RL loading is presented in Figure 12.

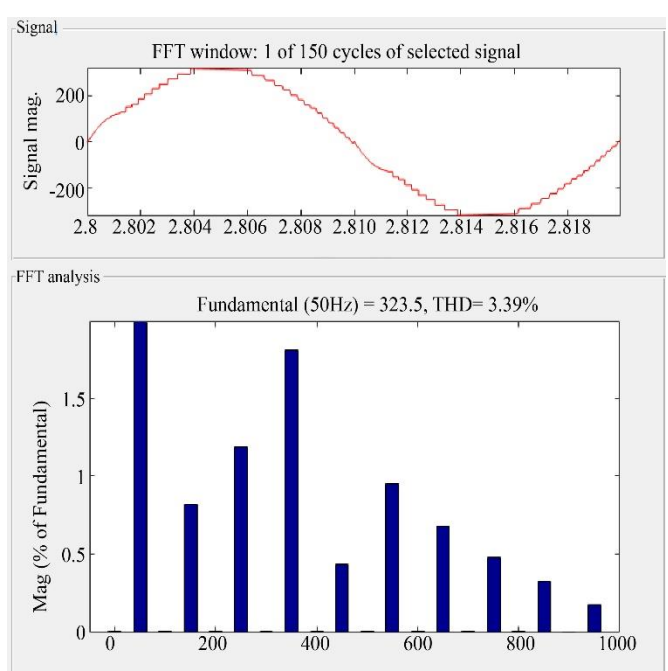
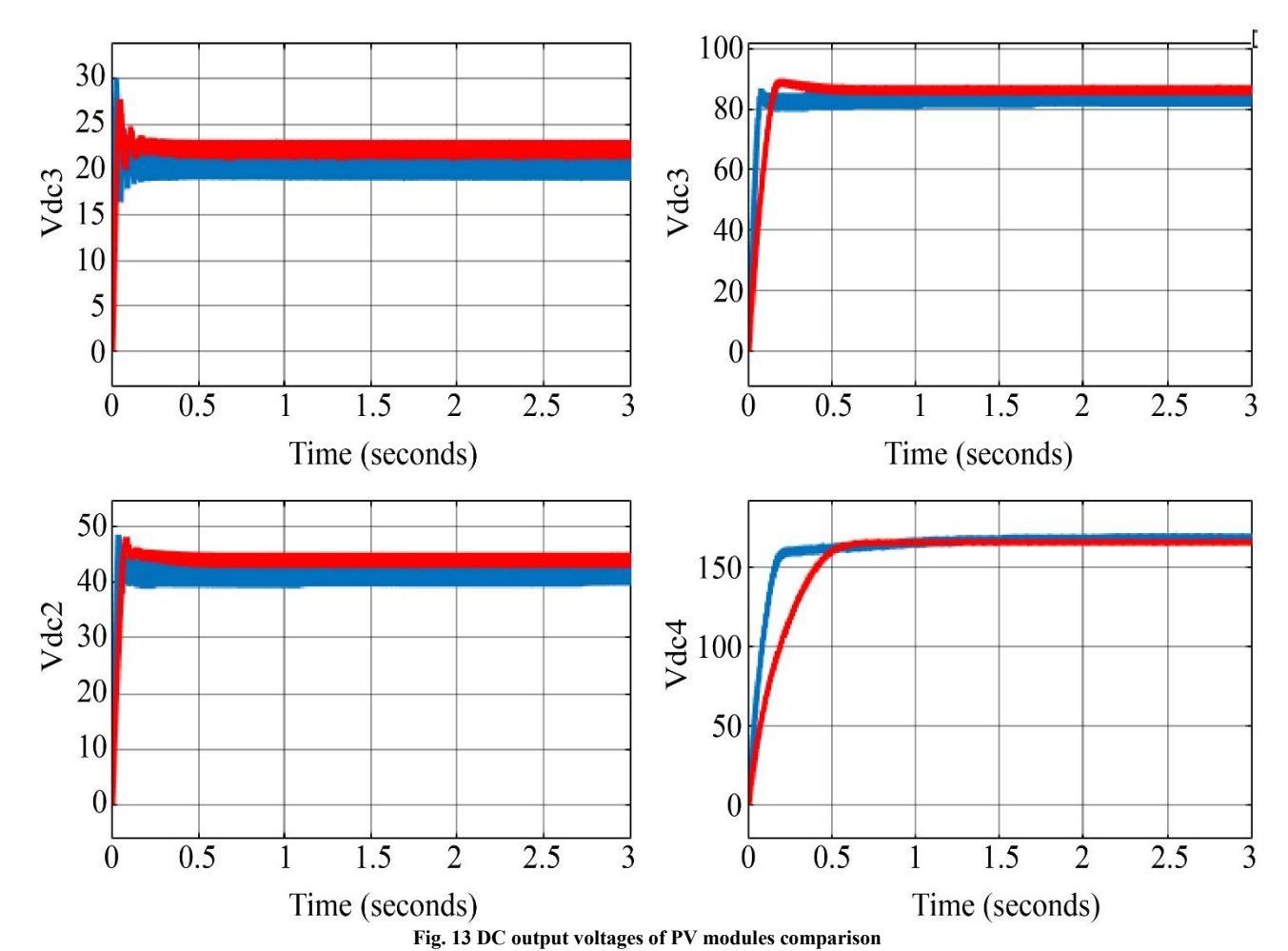


Fig. 12 FFT analysis of inverter voltage with resistive and inductive load

As shown in Figure 12, the THD of the inverter output voltage with the inductive load is recorded at 3.39%, which remains nearly identical to the value obtained with only a resistive load. To further enhance system performance, the PV

modules are integrated with a fuzzy logic-based MPPT controller, enabling improved power extraction and reduced voltage ripple. Figure 13 illustrates the comparison of the DC output voltages of the PV segments under P&O and fuzzy MPPT techniques. As observed from the graphs in Figure 13,

the DC voltage ripple of the PV modules is significantly reduced when operated with the fuzzy MPPT technique. This improvement is attributed to the smoother tracking of the duty ratio, which minimizes ripple content and enhances the voltage regulation of the boost converter.



2100
2000
1900
1900
1700
1600
0 0.5 1 1.5 2 2.5 3
Time (seconds)

Fig. 14 Inverter output power comparison

In addition to reducing DC voltage ripple, the fuzzy MPPT also enhances tracking speed. As shown in Figure 14, the power extracted from the PV modules stabilizes at 2.2 s when using the conventional P&O MPPT, whereas with the fuzzy MPPT, it settles much faster at 0.6 s. Furthermore, the fuzzy MPPT achieves a higher total power extraction, delivering approximately 60 W more than the conventional method.

4.2. Case 2: Variable Irradiation for All PV Panels

In this scenario, solar irradiation varies at different time intervals, directly influencing the inverter voltages and power output. The simulation is extended to 3 seconds, with irradiation initially set at 1000 W/m². At 1 sec, the irradiation level reduced to 500 W/m², and at 2 sec, it increased again to 700 W/m², causing fluctuations in the DC voltages. The corresponding inverter output voltage during the irradiation drop (between 1 sec and 2 sec) is illustrated in Figure 15.

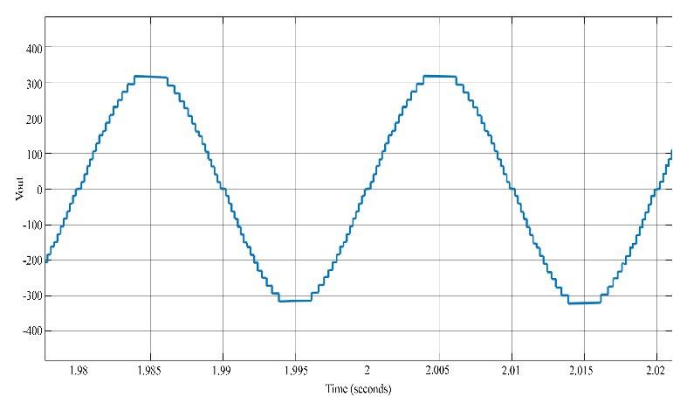


Fig. 15 Inverter output voltage with variable irradiation

Due to the voltage regulator-based MPPT technique, the inverter is able to maintain a consistent voltage pattern, generating 31-level voltages even under irradiation variation. The FFT analysis of the inverter voltage at 500 W/m² irradiation is shown in Figure 16. As shown in Figure 16, the THD of the inverter voltage is measured at 3.34%, which remains unchanged compared to the maximum irradiation condition of 1000 W/m². With varying irradiation levels, the DC output voltages of the PV modules are also analysed and presented in Figure 17. The plots provide a comparative evaluation of the DC voltages under P&O and Fuzzy MPPT techniques. It is observed that, regardless of the irradiation

condition, the Fuzzy MPPT maintains significantly lower ripple in the DC voltage compared to the conventional P&O method.

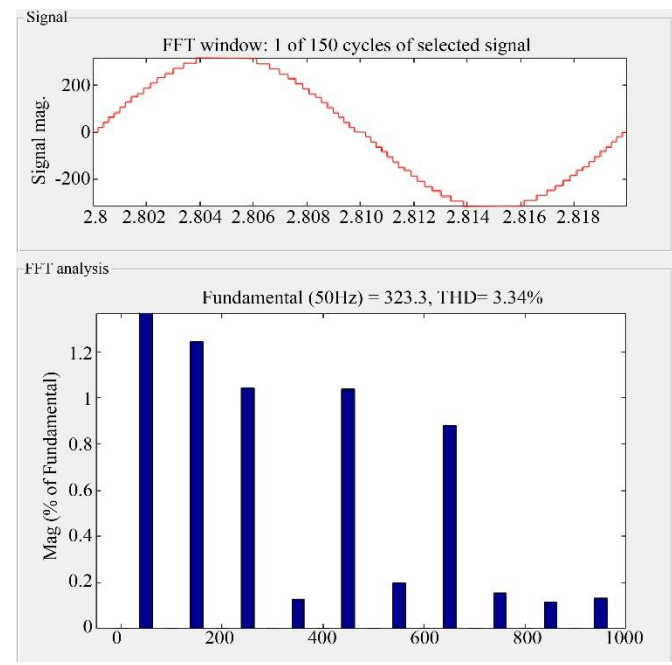


Fig. 16 FFT analysis of the output voltage with 500W/m2 irradiation

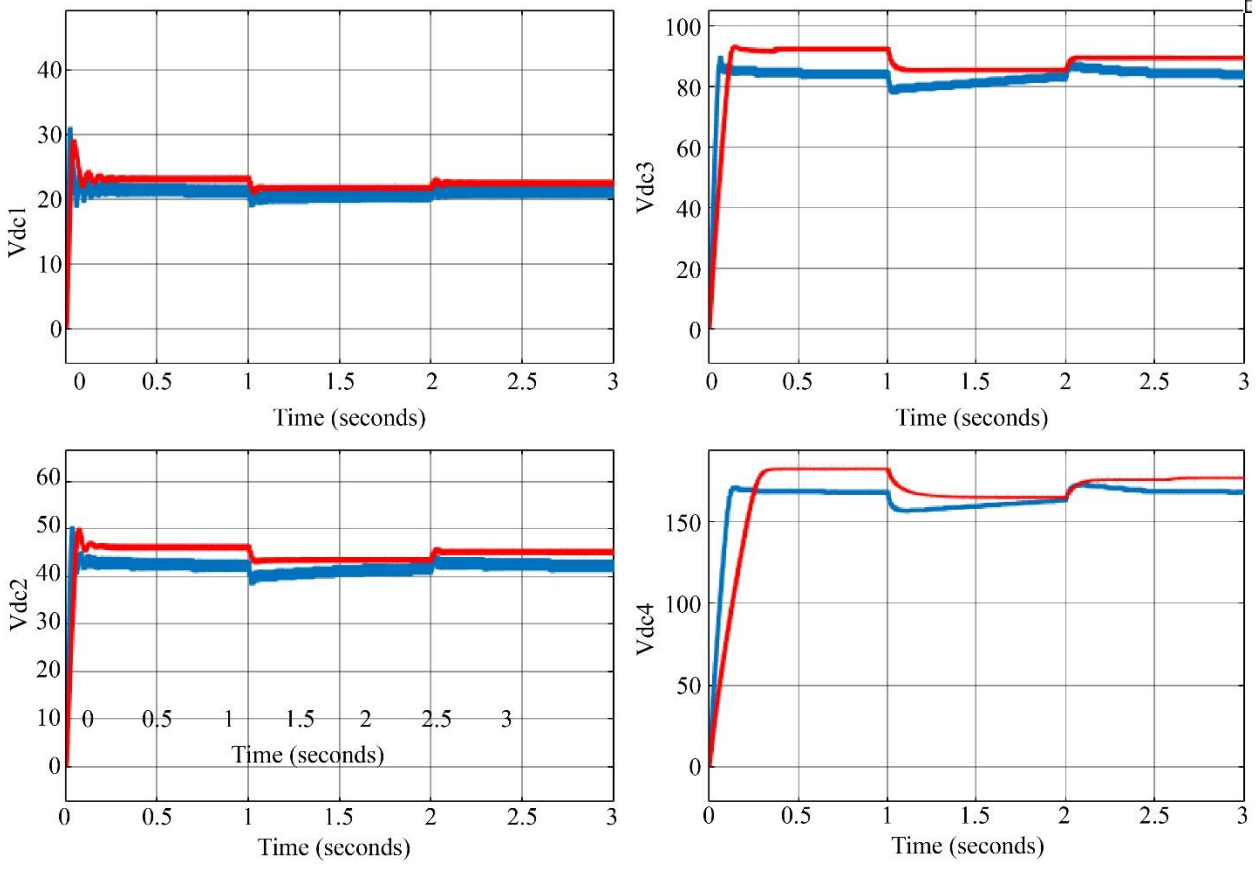


Fig. 17 DC output voltages of PV modules comparison during variable solar irradiation

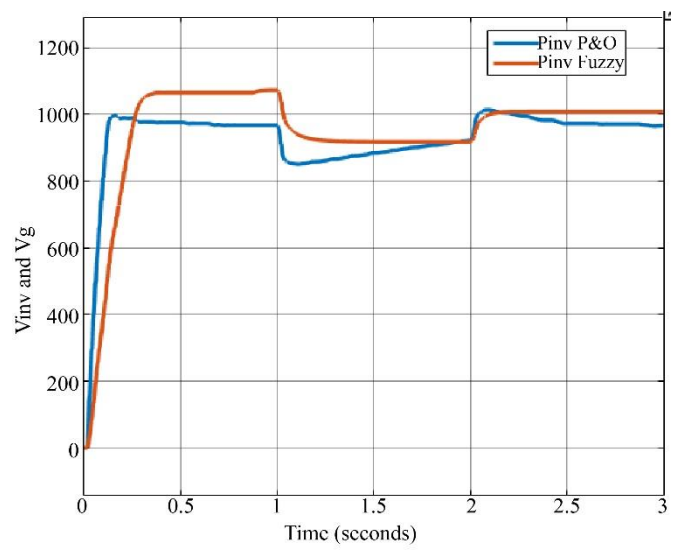


Fig. 18 Inverter output power during variable irradiation

As shown in Figure 18, the extracted power from the PV array is both more stable and higher when the modules are controlled using the Fuzzy MPPT technique. However, in both MPPT methods, the extracted power exhibits variations of up to 100 W. These fluctuations can be further minimized by integrating advanced control strategies into the MPPT for improved voltage regulation and enhanced stability.

5. Comparison and Observations

The table below represents the comparison between P&O and the Fuzzy MPPT method with respect to major components, such as maximum power tracking time, maximum power achieved, and THD. It is showing the FL-based system will produce better results compared to traditional methods like the MPPT P&O Method.

S.No.	Parameter	P&O MPPT	FUZZY MPPT	Observations with Fuzzy MPPT
1	MPPT Tracking	2.2 sec	0.6 Sec	Improved
1	time	2.2 300	0.0 500	mproved

Table 5. Comparison with the proposed FL method

1 Tracking time 2.2 sec 0.6 Sec Improved

Max.
Power Extracted 1920W 1980W Power Increased

3 THD High Low THD reduced

6. Conclusion

The design of the asymmetrical multi-level inverter for a standalone PV panel system intended for remote-area domestic load compensation has been successfully demonstrated. The inverter delivers promising performance, achieving a low voltage harmonic distortion of 3.38%, which is well within the IEEE 519-2022 standard limit of 5%. Importantly, the THD remains consistent under varying load and irradiation conditions. In addition to low THD, the DC voltages of the PV modules remain stable with reduced ripple.

A comparative analysis between P&O and Fuzzy-based voltage regulator MPPT techniques shows that the Fuzzy MPPT ensures faster power extraction and greater stability under variable irradiation conditions.

Even during sudden and significant drops in irradiation, the PV modules maintain their output at the desired reference levels with minimal ripple when operated under the Fuzzy MPPT. Overall, the proposed system proves to be an effective standalone renewable energy solution for remote areas, offering both voltage stability and reduced harmonic distortion.

References

- [1] N. Girgibo et al., "Risks of Climate Change Effects on Renewable Energy Resources and the Effects of their Utilisation on the Environment," *Energy Reports*, vol. 11, pp. 1517-1534, 2024. [CrossRef] [Google Scholar] [Publisher link]
- [2] Ahmed I. Osman et al., "Cost, Environmental Impact, and Resilience of Renewable Energy under a Changing Climate: A Review," *Environmental Chemistry Letters*, vol. 21, no. 2, pp. 741-764, 2022. [CrossRef] [Google Scholar] [Publisher link]
- [3] Yuping Shang et al., "Impacts of Renewable Energy on Climate Risk: A Global Perspective for Energy Transition in a Climate Adaptation Framework," *Applied Energy*, vol. 362, 2024. [CrossRef] [Google Scholar] [Publisher link]
- [4] Waqas Ali et al., "Design Considerations of Stand-Alone Solar Photovoltaic Systems," 2018 International Conference on Computing, Electronic and Electrical Engineering (ICE Cube), Quetta, Pakistan, pp. 1-6, 2018. [CrossRef] [Google Scholar] [Publisher link]
- [5] El Manaa Barhoumi, "Optimal Design of Standalone Hybrid Solar-Wind Energy Systems for Hydrogen-Refueling Station Case Study," *Journal of Energy Storage*, vol. 74, 2023. [CrossRef] [Google Scholar] [Publisher link]
- [6] Hussein Mohammed Ridha et al., "Optimum Design of a Standalone Solar Photovoltaic System Based on Novel Integration of Iterative-PESA-II and AHP-VIKOR Methods," *Processes*, vol. 8, no. 3, pp. 1-30, 2020. [CrossRef] [Google Scholar] [Publisher link]
- [7] Faizan Arif Khan, Nitai Pal, and Syed Hasan Saeed, Chapter 31 Stand-Alone Hybrid System of Solar Photovoltaics/Wind Energy Resources: An Eco-Friendly Sustainable Approach, Renewable Energy Systems, Academic Press, pp. 687-705, 2021. [CrossRef] [Google Scholar] [Publisher link]
- [8] Devalraju Prasad et al., "Design and Implementation of 31-Level Asymmetrical Inverter with Reduced Components," *IEEE Access*, vol. 9, pp. 22788-22803, 2021. [CrossRef] [Google Scholar] [Publisher link]

- [9] J. Gowri Shankar et al., "A 31-Level Asymmetrical Cascaded Multilevel Inverter with DC-DC Flyback Converter for Photovoltaic System," 2017 International Conference on High Voltage Engineering and Power Systems (ICHVEPS), Denpasar, Indonesia, pp. 277-282, 2017. [CrossRef] [Google Scholar] [Publisher link]
- [10] R.K. Rai, and O.P. Rahi, "Fuzzy Logic based Control Technique using MPPT for Solar PV System," 2022 First International Conference on Electrical, Electronics, Information and Communication Technologies (ICEEICT), Trichy, India, pp. 1-5, 2022. [CrossRef] [Google Scholar] [Publisher link]
- [11] Nitin Singh, and Ranjeeta Khare, "A Review Asymmetrical Multi-level DC-link Inverter for PV Energy System Based Voltage Regulator," *International Journal of Engineering Applied Science and Management*, vol. 5, no. 9, pp. 1-6, 2024. [Google Scholar] [Publisher link]
- [12] Bolla Madhusudana Reddy, P.B. Chennaiah, and J. Chinnababu, *Modelling of Symmetrical 13 Level and Asymmetrical 31 Level Generalized Cascaded Multilevel Inverters*, Modern Approaches in Machine Learning and Cognitive Science: A Walkthrough. Studies in Computational Intelligence, Springer, Cham, pp. 169-191, 2024. [CrossRef] [Google Scholar] [Publisher link]
- [13] Muhammad Najwan Hamidi et al., "Asymmetrical Multi-Level DC-link Inverter for PV Energy System with Perturb and Observe Based Voltage Regulator and Capacitor Compensator," *Journal of Modern Power Systems and Clean Energy*, vol. 9, no. 1, pp. 199-209, 2021. [CrossRef] [Google Scholar] [Publisher link]
- [14] Muhammad Najwan Hamidi et al., "Asymmetrical Multilevel Inverter-Based PV System with Voltage Feedback Control: An Experimental Validation," *Applied Science*, vol. 12, no. 7, pp. 1-21, 2022. [CrossRef] [Google Scholar] [Publisher link]
- [15] M. Venkateswarlu, G. Panduranga Reddy, and S. Sankara Prasad, "Single Phase Advanced Multilevel Inverter with Reduced Devices and THD for Industrial Applications," 2023 9th International Conference on Advanced Computing and Communication Systems (ICACCS), Coimbatore, India, pp. 1006-1011, 2023. [CrossRef] [Google Scholar] [Publisher link]
- [16] Gee Varghese Mathew Kurian, P. Aruna Jeyanthy, and D. Devaraj, "Efficient Evaluation of Anticipated 31-Level Inverter for Photovoltaic Energy System with Reduced Switches," *Sustainable Computing: Informatics and Systems*, vol. 36, 2022. [CrossRef] [Google Scholar] [Publisher link]
- [17] Kifayat Ullah et al., "Fuzzy-Based Maximum Power Point Tracking (MPPT) Control System for Photovoltaic Power Generation System," *Results in Engineering*, vol. 20, pp. 1-10, 2023. [CrossRef] [Google Scholar] [Publisher link]
- [18] B. Bendib et al., "Advanced Fuzzy MPPT Controller for a Stand-alone PV System," *Energy Procedia*, vol. 50, pp. 383-392, 2014. [CrossRef] [Google Scholar] [Publisher link]
- [19] Carlos Robles Algarín, John Taborda Giraldo, and Omar Rodríguez Álvarez, "Fuzzy Logic Based MPPT Controller for a PV System," *Energies*, vol. 10, no. 12, pp. 1-18, 2017. [CrossRef] [Google Scholar] [Publisher link]
- [20] S. Narendiran et al., "Fuzzy Logic Controller based Maximum Power Point Tracking for PV System," 2016 3rd International Conference on Electrical Energy Systems (ICEES), Chennai, India, pp. 29-34, 2016. [CrossRef] [Google Scholar] [Publisher link]